Experimental Investigation of Numerical Design Method for Point-Supported Glass

Joshua Schultz, S.M.ASCE[1]; Douglas Stahl, P.E., Ph.D.[2]; and Christian Stutzki, P.E., Ph.D., M.ASCE[3]

Abstract: Calculating stresses in structural glass components is essential for design, but is especially complex for customized components like point-supported glass (PSG) balustrades. Stress concentrations are introduced at the discontinuities of the plates precisely where boundary conditions elicit maximum field stresses. Further complicating design, most published stress data for glass components are based on annealed, edge-supported glass experiments—with limited applicability to fully tempered (FT), PSG applications. This article presents experimental and numerical results for a typical application of FT glass as a PSG structural balustrade. Strain data from six FT, monolithic glass balusters loaded to both service and ultimate conditions indicates 55.2-MPa stresses at service load and 155-MPa stresses at failure. Additionally, a design algorithm is developed, using beam theory with stress concentration factors to establish preliminary thickness for use in an optimized numerical analysis to calculate stresses. Comparison of numerical and experimental data leads to the conclusion that FT, PSG balustrades are most accurately idealized by solid linear elements and translation-fixed, rotation-permitted boundary conditions at the support node. **DOI: 10.1061/(ASCE)AE.1943-5568.0000066.**

CE Database subject headings: Glass; Structural design; Ultimate strength; Numerical models; Stress distribution; Stress concentration; Laboratory tests.

Author keywords: Structural glass; Point-supported glass; Ultimate strength; Numerical models; Stress distribution; Stress concentration; Laboratory tests.

Introduction

Custom applications of structural glass flooring, stair treads, lateral supports for window walls, railings, and balustrades allow architects to create greater transparency in buildings. These applications are possible largely because of developing trends in current design: a shift from annealed to fully tempered (FT) and laminated glass, and the increase of point supports, rather than line or edge supports (Schultz 2009; Seibert 2004). Structural evaluation of point-supported glass (PSG) is complex, often relying on numerical analysis (Carre and Daudville 1999; Haldimann et al. 2008; Seibert 2004). While aesthetic consideration for more transparent facades and interiors is driving an increased use of PSG, related experimental data and design methods are not addressed adequately in building codes or standards. The preference for FT or laminated glass has existed in building codes since the International Building Code (IBC) (International Code Council 2006a), which requires laminated or FT glass for safety applications. However, current standards like the ASTM E1300 (ASTM 2007) employ design charts based on experimental data from annealed, line supported tests (Beason and Morgan 1984; Schultz 2009), and extend applicability of annealed data to FT application via simplified glass type factors. This process does not directly utilize FT data and neglects differences between annealed and FT glass (e.g., characteristics of behavior with aging, size and amount of surface flaws, and severity). Moreover, the data are based on line-supported—not PSG—tests of annealed glass (ASTM 2004, 2007). Complicating matters, the IBC has removed sections about glass design in code cycles since 2006 (as a result, International Code Council 2006a, b rather than the IBC for 2009 will be referenced).

For the specific application of glass balustrades, a designer may consider the handrail to be independently supported and acting as the load-resisting system, allowing the glass balustrade to be designed as infill glass (International Code Council 2006a, b). While this approach meets the structural requirements for load transfer, it often results in obtrusive railings that underutilize the strength of the FT structural glass. An increasingly popular alternative is to use the glass balustrade as the primary structural member to support the railing. Such designs allow handrails to be minimized, while the glass balustrade transmits all loads to the supporting structure, as shown in Fig. 1.

This article presents an efficient design procedure for FT glass balustrades that is based on (1) experimental determination of stress distributions and breaking stress for FT PSG glass balustrades; (2) comparison of numerical results with experimental data to determine the most appropriate finite-element analysis (FEA) model; and (3) creating a semianalytical method of design, which uses the Euler-Bernoulli beam theory with stress concentration factors to establish a trial thickness in conjunction with numerical analysis to determine maximum stresses and displacements.

Experimental Determination of Stresses

Introduction

As noted, current standards often employed for FT PSG glass design are based on inapplicable experimental data. The complex nature of

[1]Ph.D. Candidate, Civil Engineering, Marquette University, Milwaukee, WI 53233 (corresponding author). E-mail: joshua.schultz@marquette.edu

[2]Professor of Architectural Engineering and Building Construction, Milwaukee School of Engineering, Milwaukee, WI 53202.

[3]Professor at College of Architecture, Illinois Institute of Technology, Chicago, IL 60647.

Note. This manuscript was submitted on January 20, 2011; approved on September 8, 2011; published online on January 25, 2012. Discussion period open until February 1, 2013; separate discussions must be submitted for individual papers. This paper is part of the ***Journal of Architectural Engineering***, Vol. 18, No. 3, September 1, 2012. ©ASCE, ISSN 1076-0431/2012/3-223–232/$25.00.

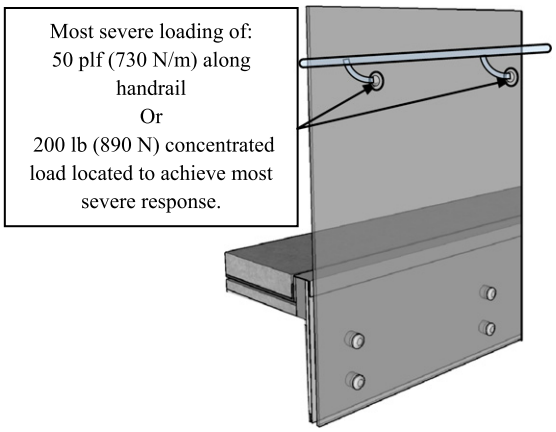

Fig. 1. Point-supported glass balustrade

stress distributions for PSG, coupled with the different material behavior between annealed and FT, prompted this experimental investigation. Existing bodies of strength data are obtained from either four-point bending or coaxial double-ring testing, both of which employ line supports and have limited applicability to glass that is truly point-supported (ASTM 2006, 2007). In an effort to establish a body of data for PSG balustrade point-support conditions, tests were designed to facilitate measurement of strains near circular holes in FT glass panels subjected to out of plane bending. Results are compared with existing strengths taken from ASTM E1300 and the Glass Association of North America (GANA) Glazing Manual (GANA 2004).

Test Setup

Setup and methodology follow the procedure outlined in detail by Schultz (2009). The glass specimens, based on a structural glass balustrade, were FT monolithic glass 610-mm wide by 1,290-mm long with a 1.59-mm edge chamfer around all sides, as shown in Fig. 2. All edges are polished. Holes for the point supports and the load application measured 25.4-mm nominal (24.4-mm actual) diameter with a 1.59-mm edge chamfer.

The thickness of the glass, measured at several locations 6.35 mm from the chamfer, was within ASTM specifications (ASTM 2007). The actual thickness of each specimen was 11.9 ± 0.1 mm. Consequently, the thickness was treated as constant in numerical modeling and analytical calculations.

The panel was supported at four locations with stainless steel through bolt fittings. Each fitting consisted of a stainless steel bolt and cap, two washers, a nylon bushing, and the steel base. The washers were a black ethylene propylene diene monomer rubber with a durometer of A60. The glass was secured by uniform pressure to both surfaces applied by the stainless steel cap as the flat head bolt was tightened. The only movement in the support was because of compression deformation of the EPDM washer and nylon bushing, and therefore it was considered fixed with regard to both translation and rotation (i.e., a rigid connection).

The nylon spacers were machined to fit inside the hole with the smallest tolerance that constructability permits. Any additional clearance contributes to a stress concentration at the reduced contact area. A gap of even 2 mm between the spacer and the glass increases stresses by 66% using an aluminum extruded spacer and 39% using plastic extruded spacers (Haldimann et al. 2008).The stainless steel mounting was rigidly attached to the steel flanges of the test frame using steel plate washers and A325 structural bolts.

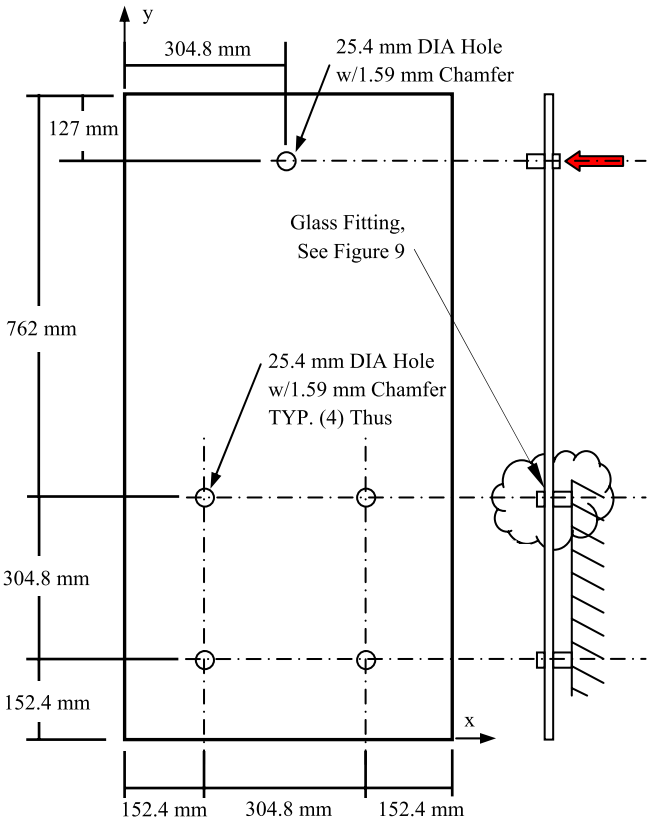

Fig. 2. Glass specimen geometry and support conditions

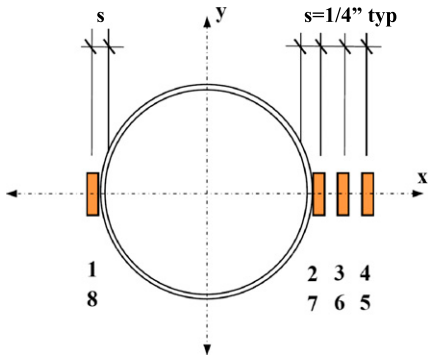

Fig. 3. Strain gauge numbering and spacing

During loading, the strains were measured at critical points on the tension surface of the glass near the topmost set of holes, as shown in Fig. 2. At both of these holes, one strain gauge was applied adjacent to the chamfer at each side of the hole. The four remaining strain gauges were placed 6.35 mm on center spacing on the exterior side of the hole, as shown in Fig. 3. Gauges were affixed with cyanoacrylate adhesive.

The EPDM washers on the tension surface of the glass were placed to avoid direct pressure from the bolted connection on the gauges.

Test Procedure

The load was applied normal to the plane of the glass specimen with a hydraulic actuator in at a rate of 14.8 N/s. The load was

J. Archit. Eng. 2012.18:223-232.

applied to the glass specimen with a connection similar to that used at the supports, mimicking a typical handrail to glass connection. A concentrated load of 890 N was established as the design load per IBC 1607.7.1.1 (International Code Council 2006b). The glass self-weight was ignored during these tests.

At point of application, the load piston was attached to the hydraulic actuator using a rotational clevis, and therefore the cantilevered portion of glass deflected the connection rotated to remain normal to the glass (Schultz 2009). Because rotation in the clevis remained small even at the extreme limits of testing, second-order effects on the results were minimal and neglected (i.e., load application remains normal to glass).

The first specimen was loaded to 890 N, held for 60 s, and unloaded through 10 cycles before being loaded to failure. The cyclic and sustained load durations in this experiment were introduced to see if there were any comparable effects in FT glass at this load and time. The remaining five specimens were loaded once with 890 N and held for 600 s before loaded to failure. The purpose of the repetitive load application and load holding was to discern if there are any effects of cyclic loading or load duration on the integrity of the glass specimen at experimental load levels. No fatigue was observed or expected because of residual surface stresses present in FT glass, as discussed by Schultz (2009). As explained by Haldimann et al. (2008), Levengood (1958), and Carre and Daudville (1999), subcritical crack growth results in a static fatigue effect in annealed glass, and ASTM testing guidelines for testing all glass require this evaluation. All data recorded at 0.5-s intervals included force at the actuator, displacement at the point of load application, and the 10 strain channels.

Experimental Results

Results include load, displacement, and strain data for the six specimens, but because the glass specimens are symmetric along one axis and the holes are spread far enough that the stress discontinuity fields are not likely to interact, the strain gauge data from each hole are treated as unique specimens. Consequently, 12 sets of strain data are given instead of six. A typical plot of load versus displacement in Fig. 4 shows the linearity of the glass specimen under load. The deflection results for each specimen are displayed in Table 1 at a service load of 890 N and the ultimate load for each specimen.

For the six specimens, the average deflection at service load is 15.2 mm, with a standard deviation of 0.5 mm. Values for the deflections at the ultimate load are based on the deflection of the specimen immediately before failure, with coefficients of variation around 10%. The deflection is measured in the direction of loading (perpendicular to the original undeformed glass plane) and at the load application point. The average deflection at ultimate load is 47.3 mm.

The strain results for Specimen 1 are typical of all the specimens. As shown in Fig. 5, the specimen is linear until failure. The graph

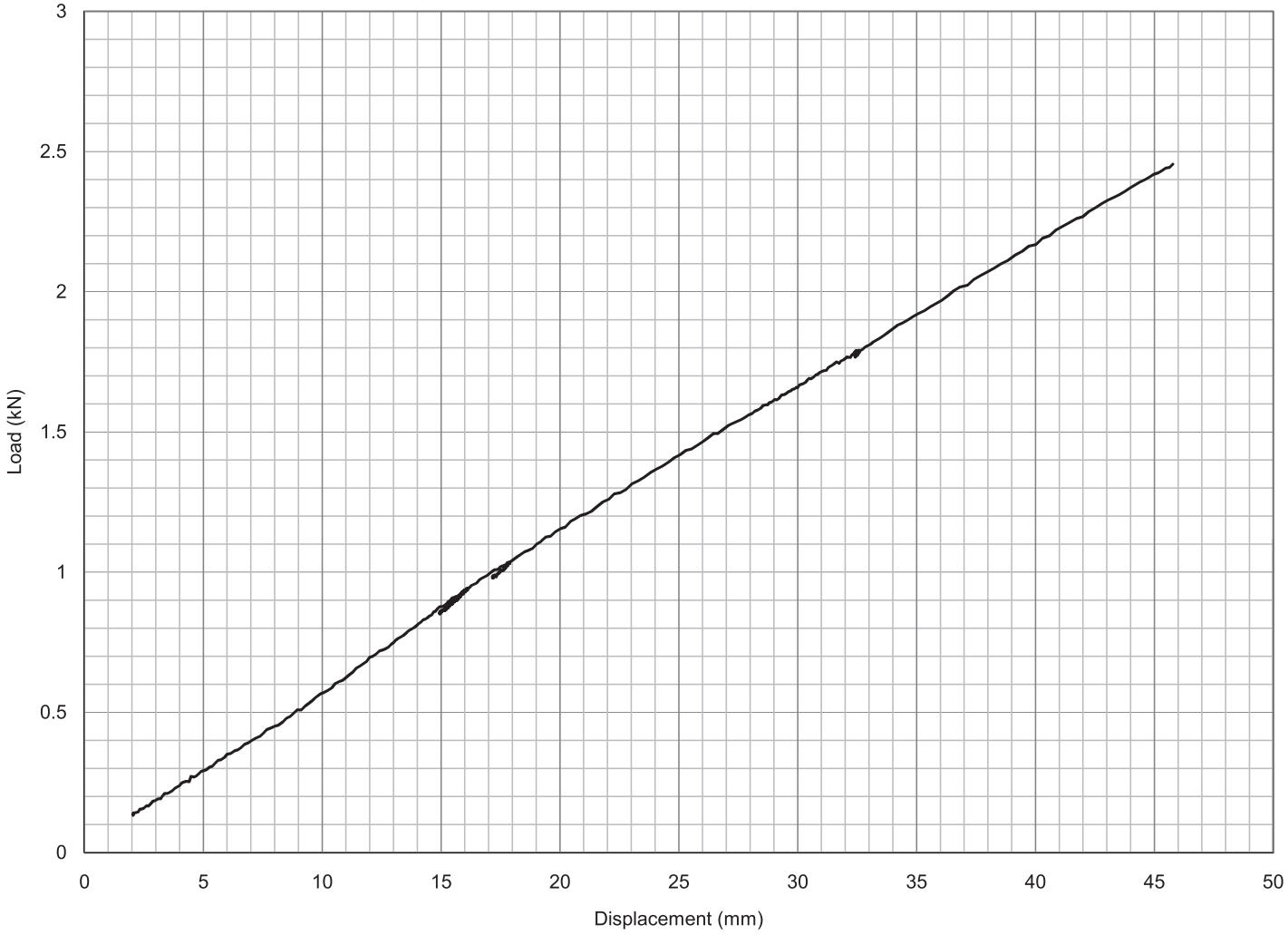

Fig. 4. Specimen 1 deflection: plot shows typical response of all specimens

J. Archit. Eng. 2012.18:223-232.

shows the elastic response of the panel to loads up to the ultimate strain.

Load duration and load cycles were observed not to have a significant impact on the strength and integrity of the tempered glass. Inspection of several aspects of the results led to this conclusion. First, the hysteresis of each strain gauge for each specimen remained tightly constricted with no pinching, indicating a lack of significant inelastic deformation. Fig. 6 provides a close look at the typical load versus strain, which highlights the consistency of the specimen to loading. Second, the specimens exhibited no strain creep when the load was held at the service level, as would be expected if the material was exhibiting static fatigue. A contributing reason for this perfectly elastic behavior is that the stresses during the tests were well below the residual surface stresses, introduced into the glass during the tempering process. These residual surface stresses resist applied tensile stresses and inhibit preexisting microcracks from opening and growing (Nielson et al. 2008; Carre and Daudville 1999). Consequentially, the engineering of tempered glass at the experimental (i.e., low) load levels does not need to consider the load duration, as long as the service loads produce stresses below the residual compression stresses of 69 MPa per ASTM C1048 at the surface of the glass (Knowles et al. 2010). However, the effect of surface stresses (present in FT) on microcracks remains an open area of investigation. Finally, the ultimate strains did not show signs of variability from specimen to specimen that could be attributed to the different load levels, durations, and cycles. Average strains of the specimens are shown in Fig. 7.

Table 1. Deflection Results

	Deflection at service load $P = 890$ N	Ultimate load and deflection	
Specimen	δ (mm)	P (N)	δ (mm)
1	15.00	2,455.00	45.70
2	15.70	2,660.00	50.50
3	16.00	2,216.00	41.10
4	14.70	2,714.00	52.30
5	15.00	2,293.00	43.20
6	15.00	2,698.00	50.80
Average (mm)	15.20	2,506.00	47.30
Standard deviation (mm)	0.51	217.38	4.59
Coefficient of variation (%)	3.33	8.67	9.71

Calculation of stress, σ_x, from strain is based on Hooke's law, where E is the modulus of elasticity for tempered glass; 71.7 GPa, and ε is the strain in experimental specimen, as provided in Fig. 7. The stresses, σ_x, for each specimen are provided in Table 2 for both the ultimate and service ($P = 890$ N) load conditions. The 12 sets of

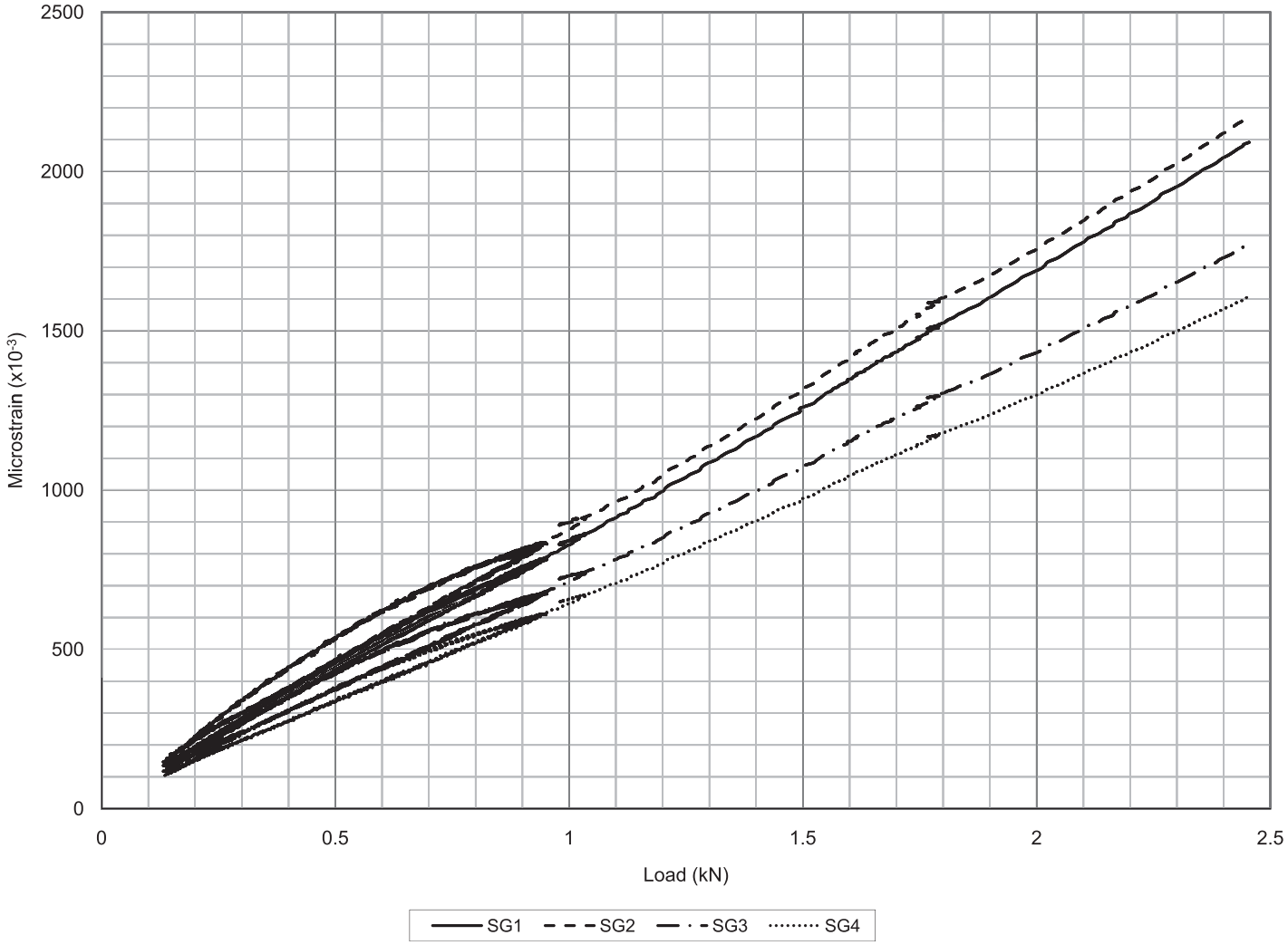

Fig. 5. Specimen 1 load versus strain: plot shows typical response of all specimens

J. Archit. Eng. 2012.18:223-232.

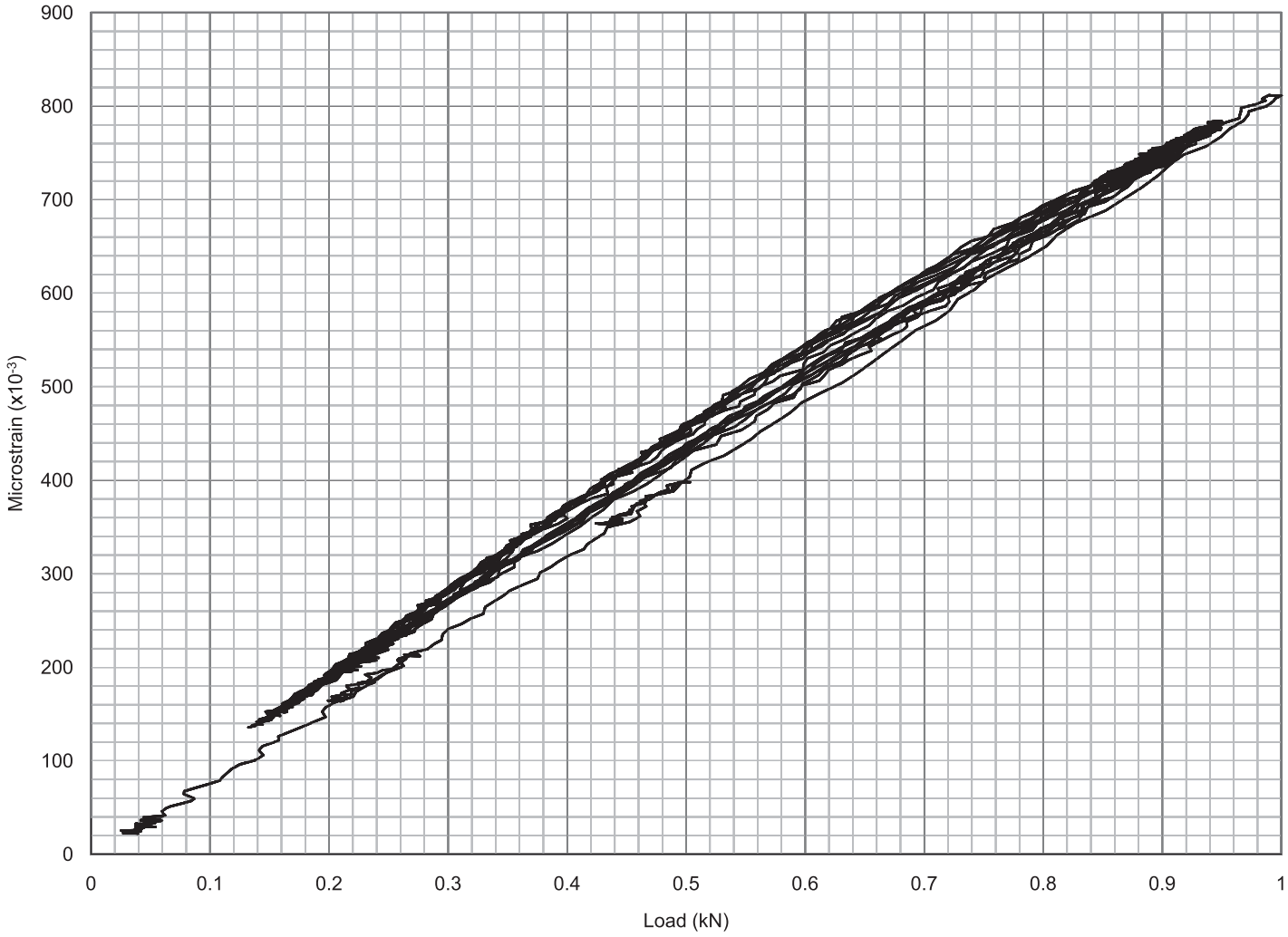

Fig. 6. Specimen 1 hysteresis: plot shows typical response of all specimens

strain data are consistent; accordingly, the average data is used in Fig. 7.

The stresses, as derived from experimental strains, at service load are compared with the allowable stresses, as established by the ASTM E1300 (ASTM 2007), American Architectural Manufacturer's Association (2008), and GANA (2004) standards. The GANA standard provides stress limits based on the type of glass application. According to the GANA (2004) manual, the allowable stress for tempered glass is 77.2 MPa for a 60-s load duration and 66.9 MPa for 600-s load duration. The experimental results provide an average peak stress (at service load) of 52.2 MPa for the 60-s load duration (Specimens 1 and 2) and an average peak stress of 54.1 MPa for the 600-s load duration (Specimens 3–12). Both of the experimental results are well below the allowable stresses.

Numerical Analysis

Overview of Analysis

The FEA is performed using the Simulia Abaqus CAE Standard software package with three-dimensional brick elements. Despite occasional use in design, plate or shell elements were not considered because of their inability to properly capture the stress peaks and distribution through the balustrade thickness. However, one plate element model was included for comparison.

The numerical analysis for this specific application is highly dependent on (1) the mesh and type of elements and (2) the interaction of materials at the boundary conditions (i.e., through-bolt supports). Consequently, this investigation relies on the authors' previous experience to preselect an appropriate mesh size and focus on the modeling of the boundary conditions and comparison of peak stresses at the holes with experimental results.

Mesh Properties

The authors' previous experience with mesh patterns and convergence allows for several conclusions regarding the mesh for PSG supports (Knowles et al. 2010). For FT glass balustrades 12- to 20-mm thick with support holes 20–28 mm in diameter, the optimal field mesh is determined to be a 25-mm mesh over the face of the specimen with two elements through the thickness, with a maximum element aspect ratio of 1:7 throughout the field. Near the hole, the mesh density consists of four elements through the thickness and has elements with maximum aspect ratios of 1:1. The finer mesh extends to a diameter of 100 mm. Full integration and default hourglass controls are used for the elements. The optimal mesh is based on convergence of stress results.

J. Archit. Eng. 2012.18:223-232.

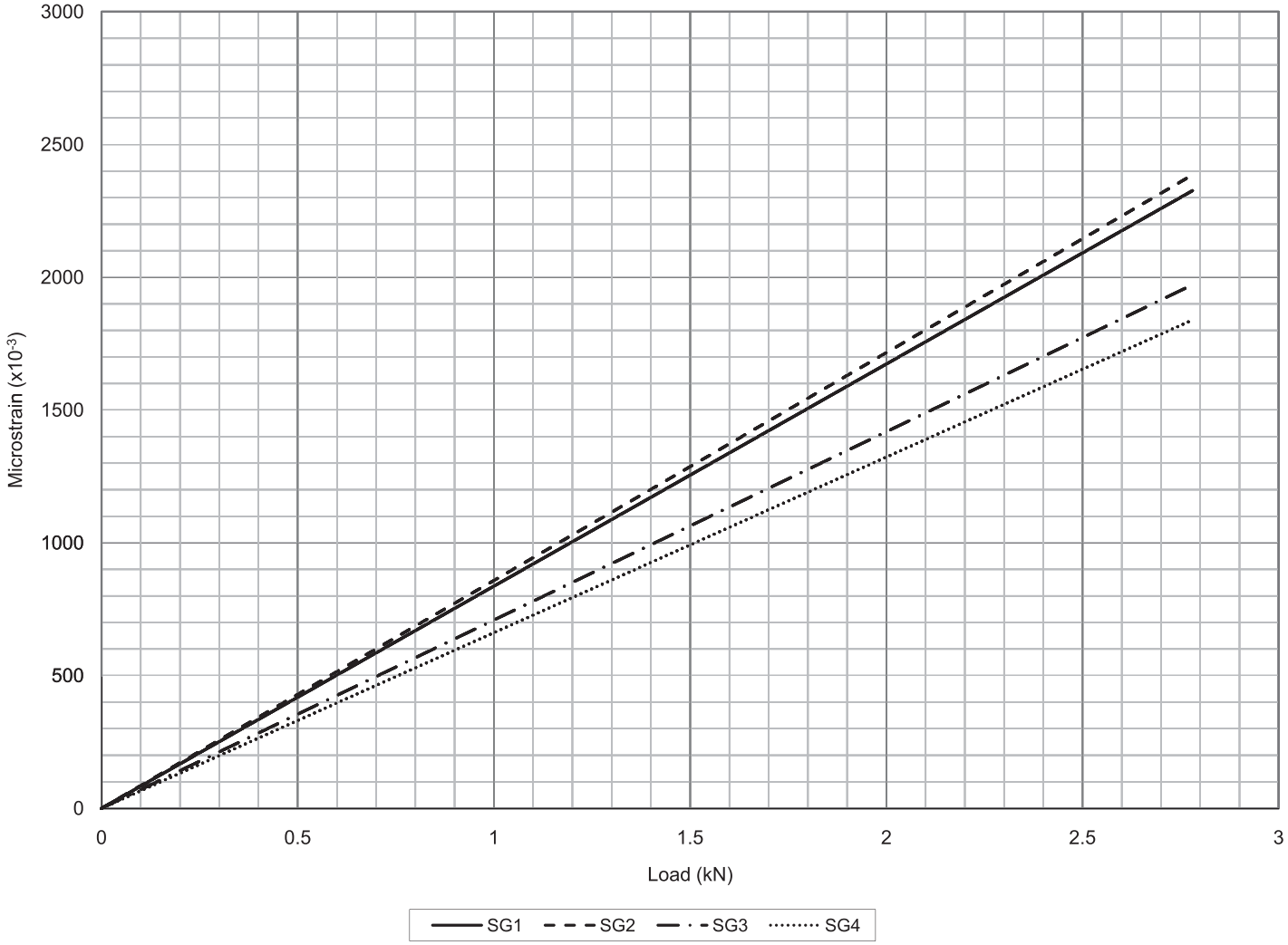

Fig. 7. Average strain versus load for all specimens

Three-dimensional solid linear elements (i.e., eight nodes) are compared with nonlinear three-dimensional solid elements (i.e., 20 nodes). Also, the number of elements across the thickness of the plate is varied (Table 3). The option of compatible modes is used throughout to accurately model bending. Various contact models (surface-to-surface) are employed (see notes in Table 3). To refine the results, the refined meshes described above were generated rather than relying on higher order elements (i.e., an h-type analysis was utilized in lieu of p-type analysis). It has been found that for similar mesh densities near the hole, the linear elements provide more accurate results than the quadratic elements when compared with experimental data. Increased complexity of the contact between the EPDM washers and glass surface near the holes precipitates governing differential equations with complex boundary conditions. Such boundary conditions are difficult to satisfy with quadratic elements, resulting in numerical errors that are minimized using the linear elements.

Boundary Conditions

Two concerns are related to boundary conditions: the connection between the glass and the rubber washer, and the support of the model for kinematic stability in analysis, as shown in Fig. 8.

The tied-fixed model is the simpler computational model, resulting in reduced run time. A tied interaction between the glass and the washer essentially glues the two materials together by having the materials in contact share adjacent nodes, and therefore when the node moves, it affects both materials without any separation from either material. This model, however, does not account for separation of the glass and washer because of curvature. This affects the stress distributions near the washer and can lead to unrealistic increases in stresses. This boundary condition is idealized in Fig. 9, where the fixity is applied to the outer surface of the washer (as indicated by hatches) and the connection between the washer and the glass is tied (as indicated by the bold line).

The interaction-point support boundary condition more realistically models the contact properties between the glass and the washer. In preprocessing, the nodes of the adjacent materials are adjusted within a tolerance distance of each other. Then, during the iterative analysis, the nodes interact according to inputs, which create hard contact normal to the surface between the two materials and allow for slip with friction along the surface. Fig. 10 shows that the outside surface of each washer is connected to a node at the center of each hole. This node serves as the reference point for the external boundary conditions.

To provide minimal kinematic support, boundary conditions are applied uniquely to the central node at each hole. From right to left and top to bottom, the boundary conditions (BCs) are as follows: the node at Hole 1 is restrained in each direction of x, y, and z; the node at Hole 2 is restrained in both y and z; the nodes at Holes 3 and 4 are restrained in only the z-direction.

J. Archit. Eng. 2012.18:223-232.

Table 2. Stress Results

	σ (MPa) at service load P = 890 N				Ultimate load P (N), σ (MPa)				
Strain gauge	1	2	3	4	P	1	2	3	4
Specimen 1	52.70	56.80	46.00	41.50	2,455.00	150.00	155.80	127.00	115.10
Specimen 2	51.7	54.90	45.90	42.10	2,455.00	146.90	150.60	126.40	116.60
Specimen 3	53.90	57.60	45.20	41.10	2,660.00	166.20	176.70	137.60	125.30
Specimen 4	52.20	54.00	45.50	41.40	2,660.00	164.70	161.60	136.70	125.40
Specimen 5	56.10	56.70	46.50	42.10	2,216.00	137.00	139.50	114.40	103.90
Specimen 6	54.20	55.70	49.70	43.00	2,216.00	133.50	136.10	121.60	105.60
Specimen 7	50.00	50.00	42.20	44.00	2,714.00	164.00	163.30	137.50	141.50
Specimen 8	50.10	51.70	47.20	42.40	2,714.00	165.20	167.80	152.00	138.00
Specimen 9	51.90	51.30	42.80	39.10	2,293.00	136.90	134.40	112.50	103.00
Specimen 10	52.80	54.80	45.50	41.70	2,293.00	141.50	143.60	119.50	110.30
Specimen 11	51.90	53.60	44.80	40.10	2,698.00	163.90	163.00	137.00	124.20
Specimen 12	49.00	52.60	44.00	40.30	2,698.00	159.90	164.60	138.30	126.80
Average (mm)	52.20	54.10	45.40	41.60	2,506.00	152.50	154.80	130.00	119.60
Standard deviation (mm)	1.97	2.39	1.98	1.33	207.11	12.86	13.73	11.73	12.76
Coefficient of variation (%)	3.77	4.42	4.35	3.19	8.26	8.43	8.87	9.02	10.67

Table 3. Finite-Element Analysis Inputs and Results

Case	δ_{max} (mm)	δ at load (mm)	Field stress (MPa)	Maximum stress (MPa)	Global mesh (mm)	Elements over thickness	Element type	Geometric order	Method
1	23.6	18.3	20.2	52.7	25.4	2	Solid	Linear	a
2	18.3	14.2	24.3	54.2	25.4	4	Solid	Linear	a
3	20.6	16.0	25.9	72.6	25.4	2	Solid	Quadratic	a
4	20.3	16.0	29.1	77.8	25.4	2	Solid	Quadratic	a
5	23.4	18.3	28.5	75.5	12.7	3	Solid	Quadratic	a
6	23.4	18.5	26.5	55.6	25.4	4	Solid	Linear	b
7	23.6	18.0	29.2	75.3	25.4	2	Solid	Quadratic	b
8	23.6	18.0	29.0	75.0	12.7	2	Solid	Quadratic	b
9	22.4	17.8	29.8	72.2	12.7	1	Shell	Quadratic	c
10	22.4	18.5	32.0	72.0	12.7	2	Solid	Quadratic	d

Note: Method a refers to chamfered hole, tied-fixed BC, full integration. Method b refers to chamfered hole, interaction-point support properties: tangential rough and normal default hard allow separation after contact, four node point supports, full integration. Method c refers to no chamfer hole, interaction-point support properties: tangential rough and normal default hard allow separation after contact, four node point support. Method d refers to chamfered hole, interaction-point support properties: tangential rough and normal default hard allow separation after contact, four node point support, full integration.

Summary of Finite-Element Analysis Models and Results

Six different models are analyzed to determine which model is the most accurate idealization of experimental support conditions and stress distributions. Because stress distributions are important in PSG design, both location and magnitude of stresses are examined. Not only do the maximum principal stresses need to be accurate, but the stress distributions need to follow the expected pattern through the glass specimen. The maximum principal stresses are examined, because in a brittle material this is the best predictor of failure, barring a detailed map of flaws where applied stresses may lead to crack growth and failure.

FEA resulted in two basic types of stress distributions. The first typical distribution is shown in Fig. 11 and is associated with the tied-fixed boundary condition. In this case, the stress patterns are not symmetric about the x-axis, as predicted by theory of elasticity (Savin 1961; Peterson 1974). This is attributed to the tied condition between the washer and the glass. While maximum stress values do not increase, there is a shift toward the top of the hole, and therefore the location of the maximum stress is moved above the axis. as shown in Fig. 11. This is because of an unrealistic boundary constraint introduced by the complete fixity of the nodes at the surface of the washers.

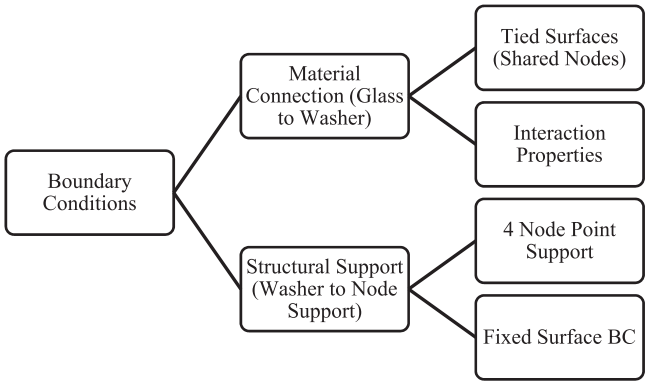

Fig. 8. Finite-element analysis idealized boundary condition options

The second type of distribution is shown in Fig. 12 and is associated with the interaction-point support surface boundary condition. In this case, the stress patterns appear to be more evenly distributed around the holes and through the field of the specimen, as shown in

J. Archit. Eng. 2012.18:223-232.

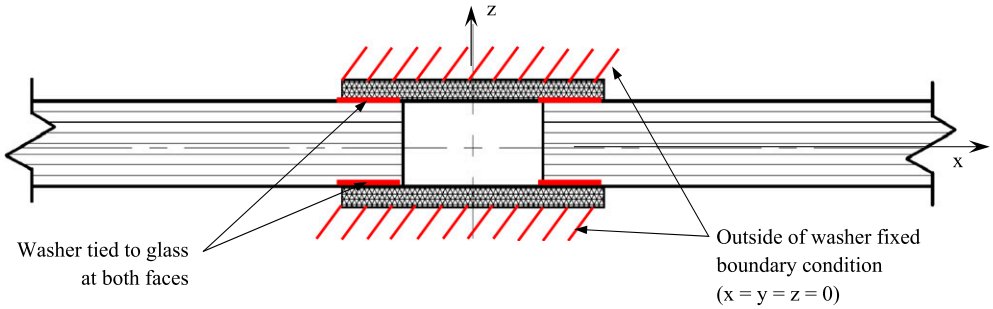

Fig. 9. Finite-element analysis tied nodes idealization of glass/washer boundary conditions

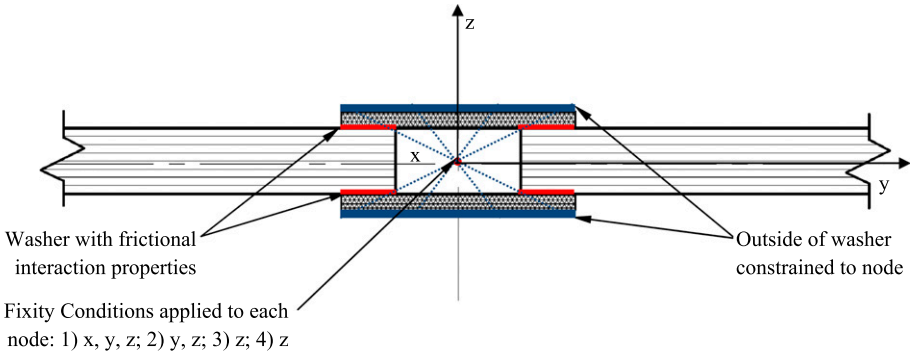

Fig. 10. Finite-element analysis contact surface interaction idealization of glass/washer boundary conditions

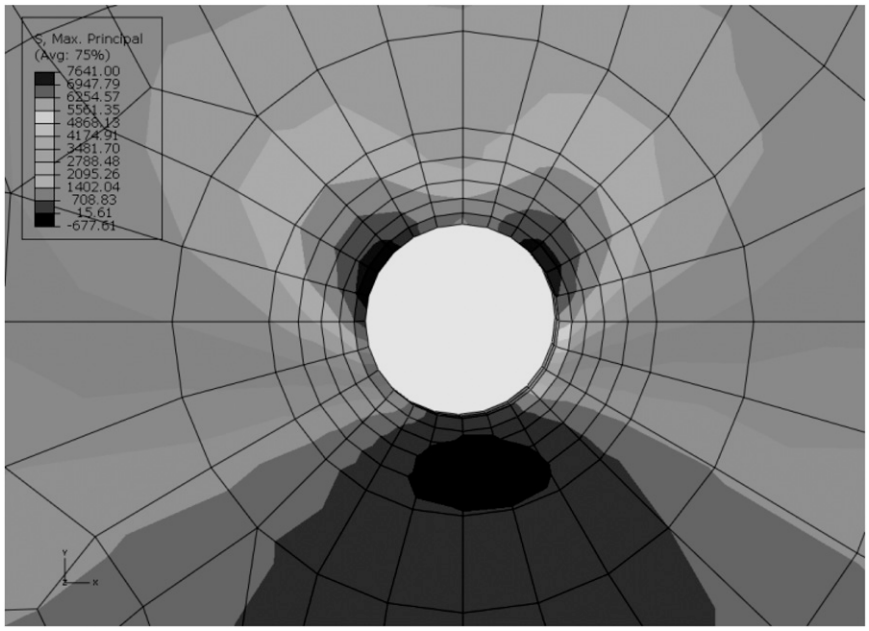

Fig. 11. Maximum principal stress distribution at hole for tied nodes idealization

Fig. 12. Such distributions are attributed to the interaction surface that is used as a connection between the surfaces, providing each surface with the ability to move independently, consistent with contact and friction requirements. The stress distributions with the interaction surfaces have the peak stresses located at the *x*-axis, as expected based on plate theory.

The summary of the FEAs is provided in Table 3.

Case 6 is selected as the most realistic FEA method by comparison of the numerical maximum strains and stresses, stress distributions, and deflections to the experimental results. Although the values for the maximum stresses of Case 2 appear closer to those of the experimental results, the stress distributions for Case 2

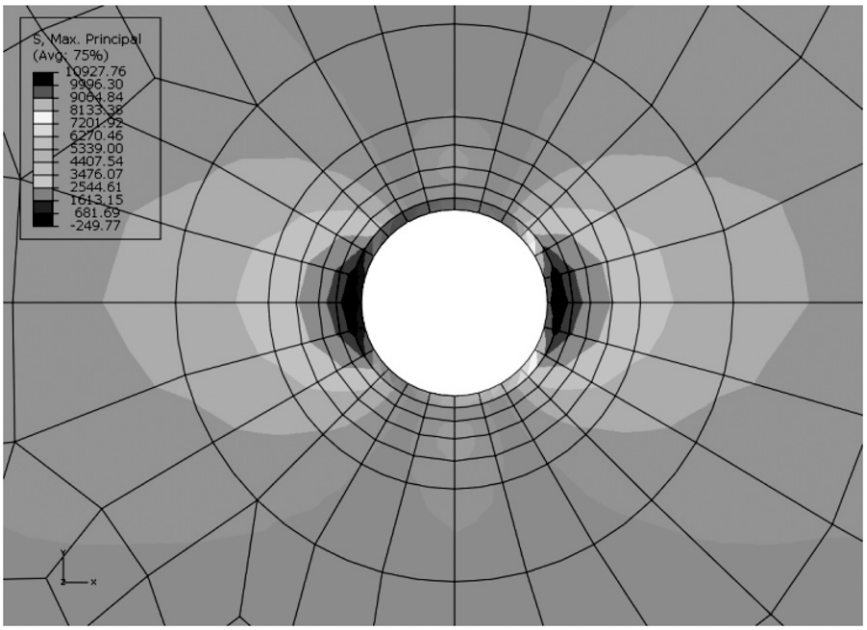

Fig. 12. Maximum principal stress distribution at hole for contact surface idealization

are unrealistic because of complete nodal fixity at the surface of the washer and the glass. While the quadratic elements do provide increased accuracy in continuum, the interaction of the through-bolt connection and the stress increases near the holes reduces the accuracy, as shown by the comparison between the numerical and experimental results. Case 6 is selected as the ideal FEA method, based on comparison of experimental and numerical deflections, stress distributions, and maximum stress values. The deflections for the service load (at point of load application) average 17.3 mm at the end of the baluster for each of the models, with the exception of the model using shell elements. As a comparison, the average deflection at the point of load application in the tests (Table 1) was 15.2 mm. The maximum principal stresses are shown in Fig. 12.

Analytical Determination of Initial Thickness

As an initial step for the design process, a simplified analytical calculation is employed to determine a trial glass thickness. The thickness is obtained by solving a Bernoulli beam equation for the thickness using an adjusted stress. For plates that have a width (L) to height (a) ratio less than four, either a beam or plate theory can be applied to determine a representative field stress (Holl 1937; Jarmillo 1950). The resultant field stress is then modified using the appropriate stress concentration factor, K, which is defined as the ratio of $\sigma_{max}/\sigma_{nom}$. The applied loading will also result in an out-of-plane shear stress (because of the support bearing) in the area of the washer. However, these stresses are an order of magnitude lower than the in-plane stresses and are neglected for these calculations.

One method of determining a stress concentration factor is to apply the research of Savin (1961) with respect to stresses around holes when bending thin plates

$$K = \{1 - [2(1 + \nu)]/(3 + \nu)\}$$

The largest value is predicted to be located at 90° from the y-axis (as confirmed in the stress distribution shown in Fig. 12). For glass with a Poisson's ratio of 0.22, the stress concentration factor, K, is 1.758.

The field stress calculations are based on modeling the baluster as a cantilever beam with a length measured from the fixity at the top set of fasteners

$$\sigma_{field} = (c \times M_{max})/I$$

where c = one half the thickness (t), the maximum moment M_{max} = applied force (P) multiplied by the length (l), and I = moment of inertia.

Introducing the equation for the moment of inertia, the maximum moment and rearranging the equation provides the following equation for plate thickness (h):

$$h = \left(\frac{6Pl}{0.25bK\sigma_{field}}\right)^{1/2}$$

The value of b is associated with a plate width conservatively determined as the baluster width, excluding the hole diameters. The value for the stress is obtained using 25% allowable glass stress (GANA 2004) and multiplying by the stress concentration factor of 1.758. For the baluster used, the calculation provides

$$h = \left[\frac{(6)(890\ \text{N})(635\ \text{mm})}{(559\ \text{mm})(1.758)(0.25)(77.2\ \text{MPa})}\right]^{1/2} = 13.3\ \text{mm}$$

Using this preliminary thickness and Table 4 from ASTM E1300, the initial selection for glass thickness is between 11.91 and 15.09 mm. This initial thickness should now be verified with appropriate numerical methods.

Summary and Conclusions

Design of FT PSG offers challenges to the engineer because of material behavior, complex stress distributions and concentrations, and ambiguity in codes and standards. This article presented experimental

J. Archit. Eng. 2012.18:223-232.

stress-strain data for a typical application and selected a converged FEA for comparison. The experimental data, FEA study, and analytical calculation are intended to aid designers and focus future experimental and FEA studies.

The experimental results show that the bending strength of FT glass balusters does not demonstrate time-dependent behavior under the experimental load and under experimental durations of 600 s and shorter.

Averaged experimental results show the maximum principal stress at service load is 55.2 MPa, while the maximum principal stress at failure is about 151.7 MPa. The measured experimental deflection at the point of load application is 15.2 mm, lower than the selected FEA deflection (17.4 mm).

The manual calculations for the determination of trial thickness can accurately employ beam theory for balustrades with width-to-height ratios (L/a) less than or equal to 4. If the ratio is greater than 4, then finite length plate theory should be used to determine the field stresses. Field stresses should be adjusted with a stress concentration factor of 1.76 for out-of-plane bending near round holes in FT glass. The boundary conditions clearly impact the stresses in the glass and lead to additional research into specifics of the connection: washer stiffness and behavior and tightness of connection have prompted investigations into analytical modeling boundary conditions of partial rigidity for improved precision.

Glass design continues to be a developing field, and there are several areas of continuing research that the authors encourage in line with the information presented here. The results are compared with both ASTM E1300 and GANA data. In addition to questionable applicability for FT PSG applications because of differences in material properties (annealed/FT) and boundary conditions (line support/PSG), these standards also require selection of multiple factors (typically probability based) for load duration, breakage probability, and in situ conditions. These factors are currently uncommented in code and relegated to engineering judgment for determination. It would be useful to investigate and tabulate the differences in comparison for variations in these parameters.

Acknowledgments

The writers would like to thank Viracon and Tri-Pyramid for their generous contributions of tempered glass and glass fittings, respectively.

Notation

The following symbols are used in this paper:

b = net cross sectional width; excludes hole;
c = distance to the neutral axis, one-half thickness of panel;
h = cross-sectional thickness of glass;
I = moment of inertia of cross section, perpendicular to plane of specimen;
K = theoretical stress concentration factor for normal (bending) stress based on linear-elastic assumptions (Hooke's law, isotropic, homogeneity, prismatic, etc.);
l = distance between point of load application and support;
M_{max} = maximum moment;
P = applied force;
σ_{max} = maximum stress; and
σ_{nom} = field stress.

References

American Architectural Manufacturer's Association. (2008). *Structural properties of glass: AAMA aluminum curtain wall series*, *Vol. 12*. American Architectural Manufacturer's Association, Des Plaines, IL.

ASTM. (2004). "Standard specification for heat treated flat glass—kind HS, Kind FT coated and uncoated glass." *C10F8-04*, West Conshohocken, PA.

ASTM. (2006). "Standard specification for flat glass." *C1036-06*, West Conshohocken, PA.

ASTM. (2007). "Standard Practice for determining load resistance of glass in buildings." *E1300-07e1*, West Conshohocken, PA.

Beason, W. L., and Morgan, J. R. (1984). "Glass failure prediction model." *J. Struct. Eng.*, 110(2), 197–212.

Carre, H., and Daudville, L. (1999). "Load bearing capacity of tempered structural glass." *J. Eng. Mech.*, 125(8), 914–921.

Glass Association of North America (GANA). (2004). *Glazing manual: 2004 edition*. GANA, Topeka, KS.

Haldimann, M., Luible, A., and Overend, M. (2008). *Structural use of glass. International Association for Bridge and Structural Engineering*, ETH Zurich, Zurich, Switzerland.

Holl, D. L. (1937). "Cantilever plate with concentrated edge load." *J. Appl. Mech.*, 4(1), A8–A10.

International Code Council. (2006a). *Glass supports*. International Code Council, Country Club Hills, IL.

International Code Council. (2006b) *Loads on handrails, guards, grab bars and vehicle barriers*. International Code Council, Country Club Hills, IL.

Jarmillo, T. J. (1950). "Deflections and moments due to a concentrated load on a cantilivered plate of infinite length." *J. Appl. Mech.*, 17(49), 67–72.

Knowles, J., Stutzki, C., Schultz, J., and Kuba, M. (2010). "Modelling of structural glass components." *Proc., SIMULIA Central Regional Conf.*, Dassault Systemes and Abaqus, Naperville, IL.

Levengood, W. C. (1958). "Effect of origin flaw charactersitics on glass strength." *J. Appl. Phys.*, 29(5), 820–826.

Nielson, J. H., Olesen, J., and Stang, H. (2008). "Experimental investigation of residual stresses in toughened glass." *Challenging Glass: Conf. Archit. Struct. Applications Glass*, Delft University Press, Amsterdam, Netherlands, 387–398.

Peterson, R. E. (1974). *Stress concentration factors: Charts and relations useful in making strength calculations for machine parts and structural elements*, Wiley, New York.

Savin, G. N. (1961). *Stress concentrations around holes*, Pergamon Press, New York.

Schultz, J. (2009). "Design of fully tempered monolithic structural glass with point supports based on ultimate stresses and stress distributions." M.S. thesis, Milwaukee School of Engineering, Milwaukee.

Seibert, B. (2004). "FE-analysis of point bearings for glass." *Glass files*, ⟨http://www.glassfiles.com/library/article829.htm.⟩ (Sep. 23, 2010).